BNL-96850-2012-CP

RELAP5 Application to Accident Analysis of NIST Research

Joo-Seok Baek, Arantxa Cuadra Gascon, Lap-Yan Cheng, David Diamond

Proceedings of the 18th Pacific Basin Nuclear Conference

Busan, South Korea
March 18 – 23, 2012

Nuclear Science and Technology

Brookhaven National Laboratory

U.S Department of Energy

DISCLAIMER

J. S. Baek, A. Cuadra, L. Y. Cheng, and D. J. Diamond

Brookhaven National Laboratory, Upton, USA

jbaek@bnl.gov, acuadra@bnl.gov, cheng@bnl.gov, diamond@bnl.gov

Abstract

Detailed safety analyses have been performed for the 20 MW D_2O moderated research reactor (NBSR) at the National Institute of Standards and Technology (NIST). The time-dependent analysis of the primary system is determined with a RELAP5 transient analysis model that includes the reactor vessel, the pump, heat exchanger, fuel element geometry, and flow channels for both the six inner and twenty-four outer fuel elements. A post-processing of the simulation results has been conducted to evaluate minimum critical heat flux ratio (CHFR) using the Sudo-Kaminaga correlation.

Evaluations are performed for the following accidents: (1) the control rod withdrawal startup accident and (2) the maximum reactivity insertion accident. In both cases the RELAP5 results indicate that there is adequate margin to CHF and no damage to the fuel will occur because of sufficient coolant flow through the fuel channels and the negative scram reactivity insertion.

1. Introduction

The reactivity transients have been calculated using a detailed RELAP5 model. The model includes the primary piping from vessel outlet to inlet, primary pump and heat exchanger, fuel element geometry and flow area, and flow channels for the six inner and twenty-four outer fuel elements. The initial operating parameters (flows, temperatures, power level and distribution, etc.) are assumed to be at their most limiting values or at the Limiting Safety System Setpoints (LSSSs). The NBSR reactor protection system logic is modeled and initiates a trip, after the appropriate instrumentation response delay, when the setpoint is reached. The limiting fuel temperature and CHFR are calculated.

In order to evaluate CHFR a post-processing of the simulation results is conducted. The Sudo-Kaminaga correlation (Kaminaga et al., 1998) is used to calculate CHF because it is considered to be an appropriate correlation for the geometry and flow of the NBSR. The correlation was developed for vertical rectangular channels in JRR-3 (Japan Research Reactor unit 3) based on CHF experiments. The CHF experiments included the effect of mass flux, inlet subcooling, outlet subcooling, flow direction, pressure, as well as the channel configuration.

A detailed three-dimensional MCNP Monte Carlo model was used to calculate the NBSR core physics input for the accident analyses, including the startup (SU) and end-of-cycle (EOC) power distributions, moderator temperature coefficient and the reactivity worths of the shim arms, beam tubes and voids (Hanson et al, 2011). This model included a plate-by-plate description of each fuel assembly, the water gap at the axial mid-plane, the beam tubes and the geometry of the shim arms. The power distributions are used to determine the local fuel conditions and the CHF ratios during the transient.

RELAP5 has been run for the following accidents: (1) the constant control rod withdrawal startup accident and (2) the maximum reactivity insertion accident. Two initial power distribution conditions are also considered in the NBSR accident analysis and they are for SU and EOC, the two most limiting points in the fuel cycle.

2. NBSR and RELAP5 Model

2.1 NBSR

The National Bureau of Standards Reactor (NBSR) achieved criticality in December of 1967 (Becker, 2000). The acronym of the reactor has remained unchanged over these 44 years, in spite of the National Bureau of Standards (NBS) changing its name to the National Institute of Standards and Technology (NIST) in 1987.

The NBSR is a heavy water (D_2O) moderated and cooled, enriched fuel, tank type machine designed to operate up to 20 MW power. It consists of an aluminum vessel filled with heavy water which also contains the core of plate-type enriched fuel elements. These elements differ from the usual plate type elements by the inclusion of an unfueled gap separating the fueled sections of each plate above and below the mid-plane of the core. A unique feature of the NBSR is the double plenum at the bottom of the vessel. These two independent concentric plenums permit the coolant flow to the inner and outer array of elements to be separately controlled.

The schematic of the NBSR reactor is shown in Figure 1. The core is contained in an aluminum tank 2.13 m (7 ft) in diameter and 4.88 m (16 ft) high. By the use of fuel elements with an unfueled center section (depicted in Figure 2), the core is split into an upper and lower section. Each of these fueled sections is 1.12 m (44 in) in diameter and 0.279 m (11 in) high. The unfueled gap between the two fueled sections is 0.178 m (7 in). The overall dimensions of the core are 1.12 m (44 in) in diameter by 0.737 m (29 in) high. The fuel plates are Al clad with meat consisting of U_3O_8 mixed with an aluminum powder, with the uranium enriched to a nominal 93% ^{235}U (high enriched uranium, HEU).

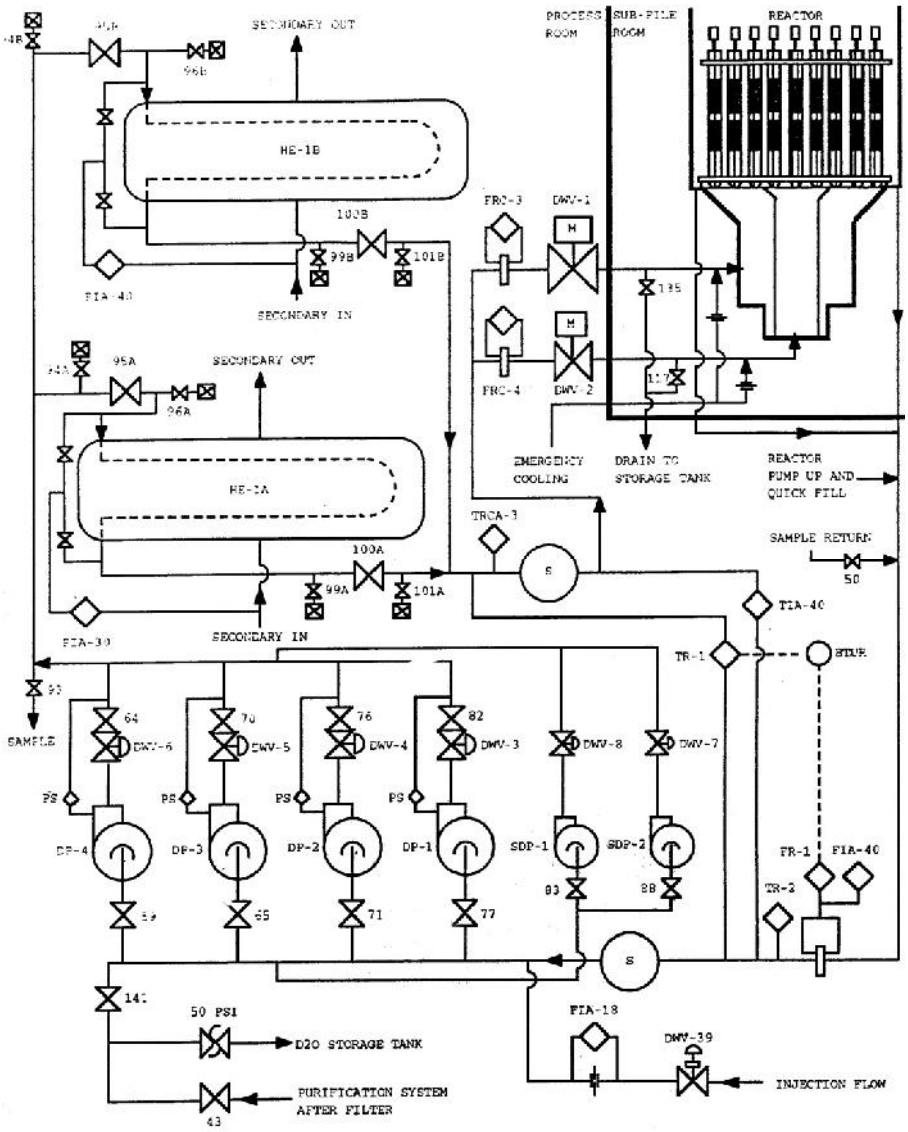

Figure 1 NBSR Primary System (Cheng et at., 2004)

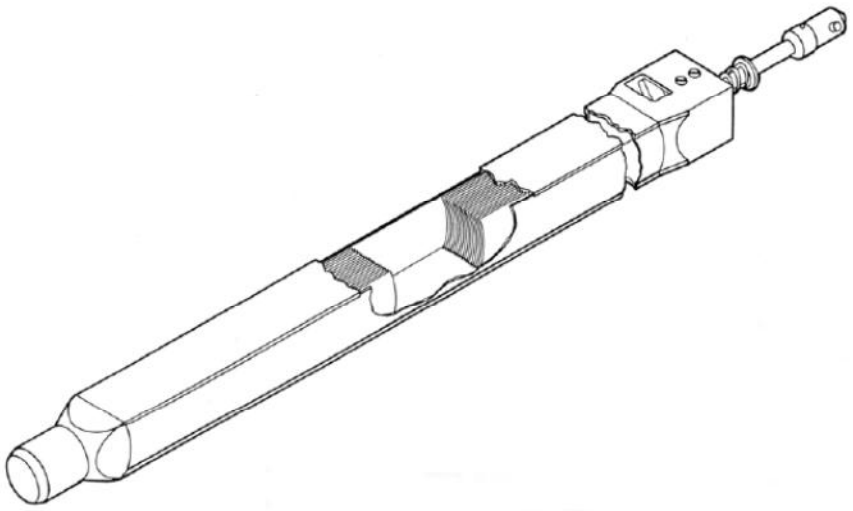

Figure 2 Cutaway Isometric Drawing of NBSR Fuel Element (Cheng et at., 2004)

The reactor's design pressure is 1034 kPa. At 20 MW the nominal inlet temperature of the D_2O coolant is 37.8ºC (100ºF) and its outlet temperature is approximately 45.6ºC (114ºF). Since most of the neutron moderation is done in the D_2O surrounding the fuel, rather than within the fuel element itself, the average moderating temperature is approximately the same as the coolant outlet temperature. For the equilibrium core at 20 MW, approximately 145 l/s (2300 gpm) of heavy water enters the inner plenum to cool the central six fuel elements, and the remaining 423 l/s (6700 gpm) is directed to the outer twenty-four fuel elements via the outer plenum.

2.2 RELAP5 Model

A detailed RELAP5 model has been developed for the NBSR. Figure 3 shows the nodal-diagram of the RELAP5 model. This figure depicts the flow channels for the six inner and twenty four outer fuel elements on the right and left sides. It is assumed in the NBSR model that the core channel flow paths are connected in parallel and the power to each channel is determined by the power distribution calculated by MCNP. Each core channel has heat structures representing the fuel plates in the lower and upper core region. A core channel may represent multiple fuel plates lumped together as an effective plate with an effective flow channel representing the flow through the plated and un-plated regions. The model also includes the primary piping from vessel outlet to inlet, primary pump and shut-down pump flow path, heat exchanger, fuel element geometry and flow area.

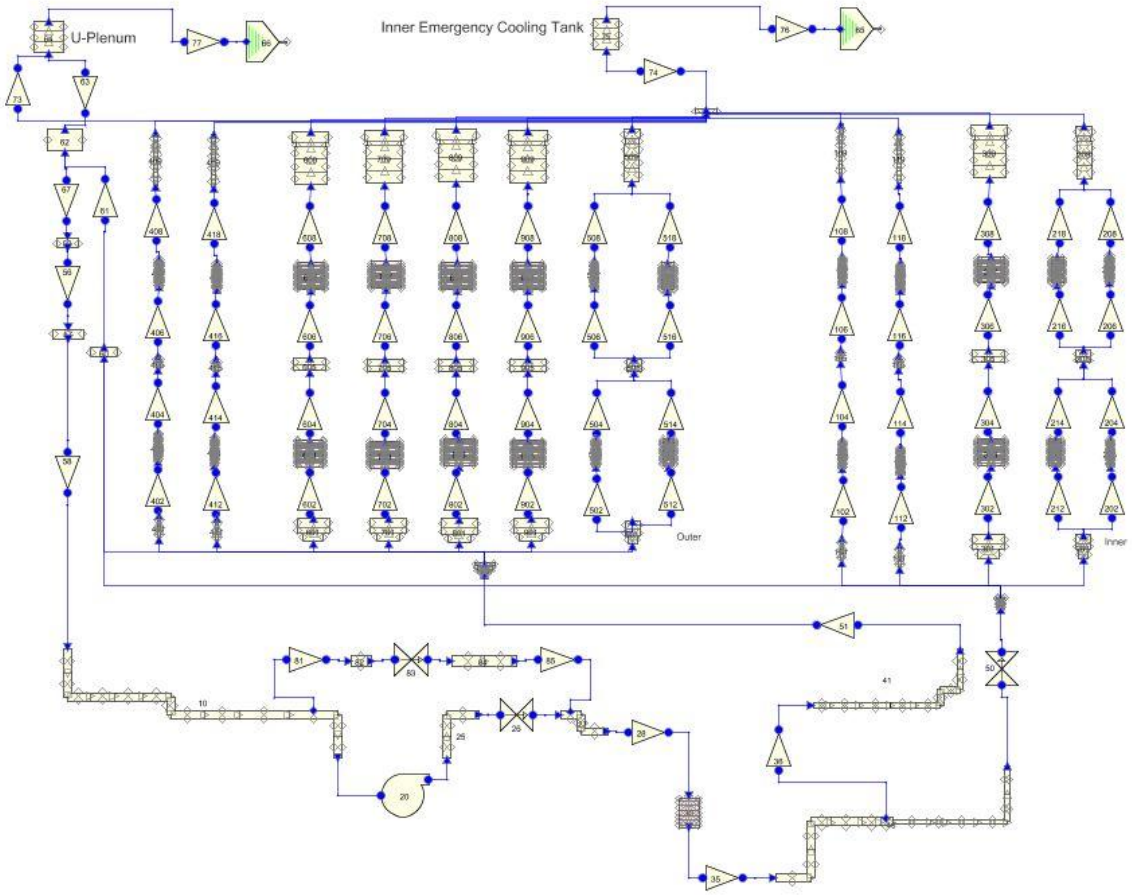

Figure 3 Nodal-Diagram of RELAP5 Model of NIST Research Reactor

Rectangular heat structures are used to represent the NBSR fuel plates shown in Figure 2. Each channel type is associated with a different heat structure and the hot elements have their own heat structures separately for the flow channels in the inner and outer core regions. The power generated by fission and fission product decay is assumed to deposit in the fuel cermet with no direct heating of the coolant assumed. Direct heating tends to lower the local power peaking in the core region and thus neglecting this effect is conservative. Since each fuel plate is cooled on both sides, it is then reasonable to model only the half thickness of a plate and double the width (i.e., heat transfer area) to give the correct wall heat flux. The cermet is modeled as a volumetric heat source and thermal energy is transferred by conduction in the fuel core (a half thickness of 0.0254 cm (0.01 in)) and the Al-6061 Temper-O cladding (a thickness of 0.0381cm (0.015 in)). The fuel core of a NBSR fuel plate has a height of 27.94 cm (11 in) and a width (flattened plate) of 6.028 cm (2.373 in). In the RELAP5 model, each NBSR fuel plate is assumed to have a heat transfer surface that has the same height but twice the width of the fuel plate.

3. Critical Heat Flux Correlation and Minimum CHFR

As mentioned earlier, the Sudo-Kaminaga correlation (Kaminaga et al., 1998) is used to calculate CHF because it is considered to be an appropriate correlation for the geometry and flow of the NBSR. The correlations proposed by Sudo and Kaminaga are mass flux and flow direction dependent and there are three separate regions, based on the dimensionless mass flux, G^*, as depicted in Figure 4. A FORTRAN program has been developed and post-processing is conducted to evaluate CHF, CHFR, and minimum CHFR for the entire core. A brief discussion about the CHF evaluation which is implemented into the FORTRAN program is presented below.

The three mass flux regions, low, medium and high, are categorized by a dimensionless mass flux:

$$G^* = \frac{G}{\lambda g \rho_g (\rho_l - \rho_g)}, \quad (1)$$

where λ is the critical wave length defined as:

$$\lambda = \left| \frac{\sigma}{(\rho_l - \rho_g) g} \right|^{\frac{1}{2}}, \quad (2)$$

and:

G: mass flux (kg/m^2.s)
σ: surface tension (N/m)
ρ_g and ρ_l: density of gas and liquid (kg/m^3)
g: acceleration of gravity (m/s^2).

The boundary values G_1^*, G_2^*, and G_3^* in Figure 1 are,

$$G_1^* = \left| \frac{0005}{\frac{A}{\rho_H} \Delta T_{subin}} \right|^{\frac{1}{0389}}, \quad (3)$$

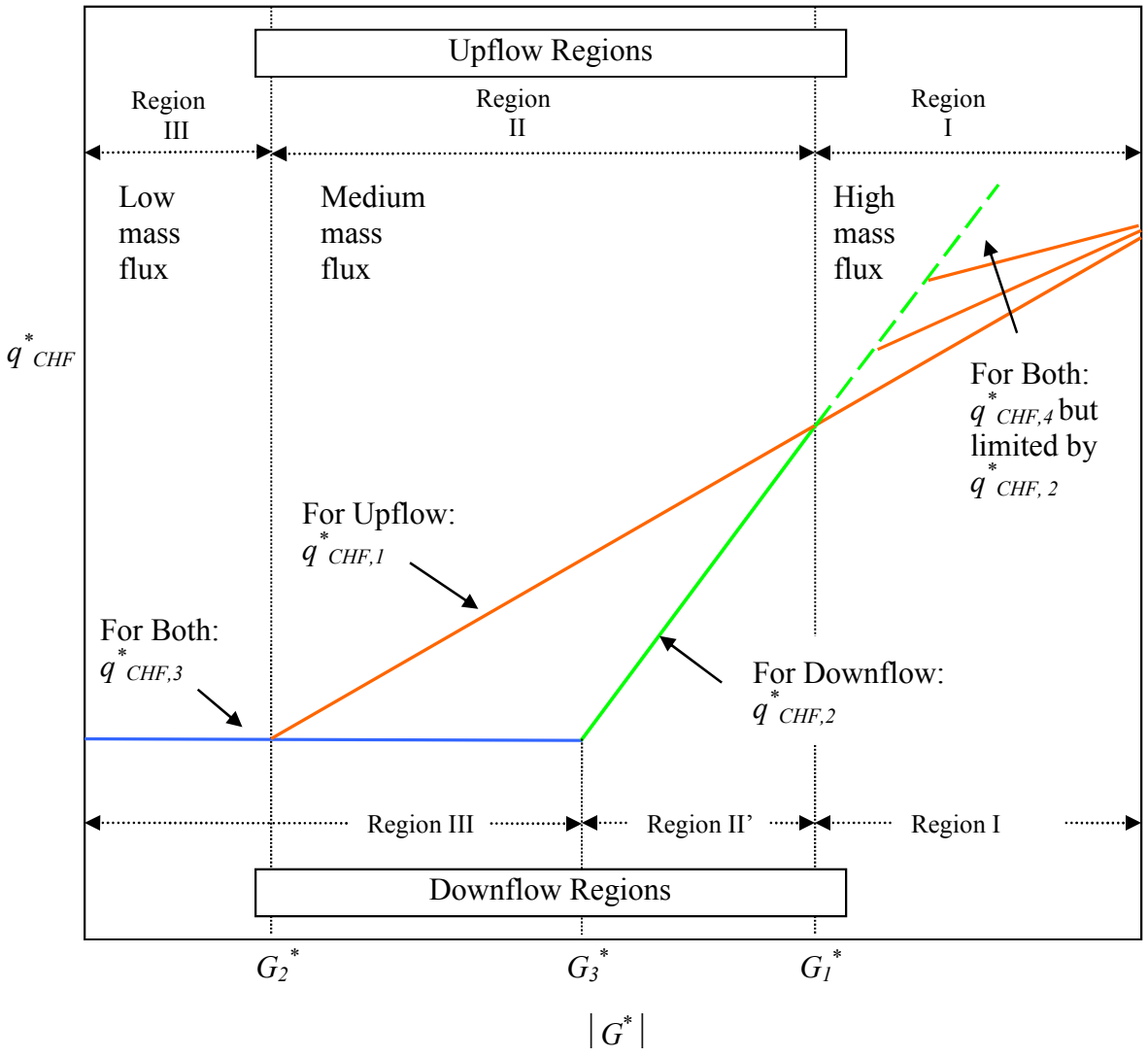

Figure 4 Sudo-Kaminaga correlation scheme (Cuadra et al., 2011)

$$G_2^* = \left| 140 \frac{A}{\rho_H} \frac{\overline{W}}{\left\{1+\left|\frac{\rho_G}{\rho_l}\right|^{025}\right\}^2} \left(1 + 3.0 \cdot \Delta T_{subin}\right) \right|^{\frac{1}{0611}}, \quad (4)$$

and

$$G_3^* = 0.7 \frac{\frac{\overline{W}}{\lambda}}{\{1+|\frac{\rho_G}{\rho_l}|^{\frac{1}{4}}\}^2} \left(3.0 + \frac{1}{\Delta T_{subin}^*} \right), \quad (5)$$

where the dimensionless subcooling at the inlet (in) or the outlet (o) is defined as:

$$\Delta T_{sub}^* = \frac{C_{pf} \Delta T_{sub}}{h_{fg}}, \quad (6)$$

and:

A: flow area (m^2)
A_H: heated area (m^2)
W: channel width of rectangular channel (m)
C_{pf}: specific heat at constant pressure of the liquid (kJ/kg.K)
h_{fg}: latent heat of evaporation (kJ/kg).

The correlation scheme proposed is applicable for both upflow and downflow:

$$q_{CHF4}^* = 0.005 |G^*|^{0611} \left(1 + \frac{5000}{|G^*|} \Delta T_{subO}^* \right), \quad (7)$$

$$q_{CHF1}^* = 0.005 |G^*|^{0611}, \quad (8)$$

$$q_{CHF2}^* = \frac{A}{A_H} |G^*| \cdot \Delta T_{subin}^*, \quad (9)$$

$$q_{CHF3}^* = 0.7 \cdot \frac{A}{A_H} \frac{\frac{\overline{W}}{\lambda}}{\{1+|\frac{\rho_G}{\rho_l}|^{\frac{1}{4}}\}^2} \cdot \left(1.0 + 3.0 \cdot \Delta T_{subin}^* \right), \quad (10)$$

where the dimensionless critical heat flux q^*_{CHF} is defined as:

$$q_{CHF}^* = \frac{q_{CHF}}{h_{fg} \sqrt{\lambda(\rho_l - \rho_G)\rho_G g}}, \quad (11)$$

The dimensionless critical heat flux for both up-flow and down-flow in Region I is predicted by q_{CHF4}^*, whereas q_{CHF1}^*, and q_{CHF2}^* are used for the up-flow and down-flow CHFs respectively in Regions II and II'. Finally, q_{CHF3}^* is applied for Region III, where the thermal limit is dictated by counter-current flow limitation (CCFL). It is, however, noted that in region I, q_{CHF2}^* limits the maximum value of q_{CHF4}^*.

Critical heat flux and CHFR are evaluated as below.

$$q_{CHF} = q_{CHF}^* \cdot h_{fg} \sqrt{\lambda(\rho_l - \rho_G)\rho_G g}, \quad (12)$$

and

$$CHFR = \frac{q_{CHF}}{q_{RELAP5}} \tag{13}$$

where q_{RELAP5} stands for the heat flux predicted by RELAP5.

4. Thermal-Hydraulic Analysis

RELAP5 simulations have been performed for postulated accidents of the control rod withdrawal startup accident and the maximum reactivity insertion accident. Two power distributions have been considered and they are the startup and end-of-cycle power distributions.

Figure 5 shows the normalized initial power distribution in hot channel at time zero. In the legend "SU" and "EOC" represent "startup" and "end-of-cycle," respectively. The power shown in Figure 5 has been normalized to the total reactor power. Hot channel heat structure stands for a fuel plate which contains the node producing the highest amount of power during the steady-state calculation. Distance of 0.0 cm stands for the dead centre of the unfueled gap between the bottom and upper fuel plates. The negative distance is measured downwardly from the centre. As shown in this figure, the two cases have different initial power distributions.

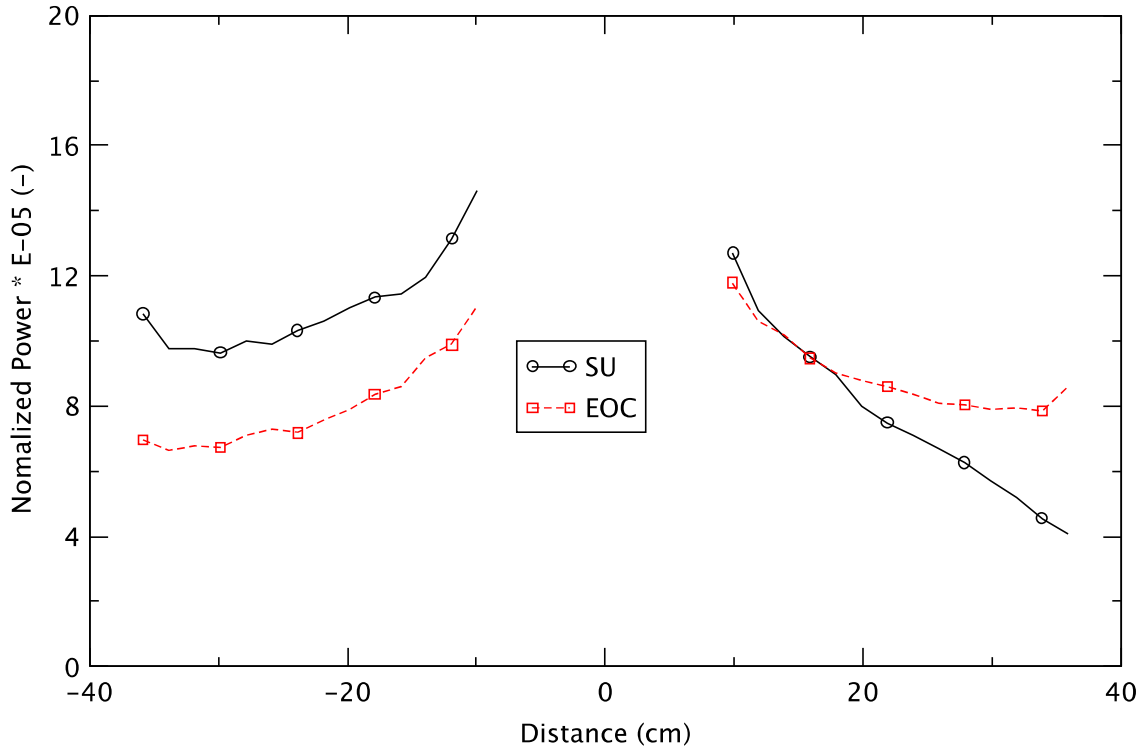

Figure 5 Initial Power Distribution in Hot Channel Heat Structure

4.1 Steady-State Conditions

RELAP5 (Ver. 3.3hj) has been run to establish the steady-state conditions of the NBSR. Table 1 shows comparison of the simulation results with the NBSR design data. The parameters are given to establish conservative initial conditions as shown in the column of remarks. The comparison of the parameters shows that the predicted values are in good agreement with the NBSR design basis ones.

Table 1 Steady-State Core Thermal Analysis Results

Parameter	SU	EOC	NBSR Data	Diff. (%)		Remarks
				SU	EOC	
Reactor power (MW)	20.4	20.4	20.4	0.0	0.0	102% of nominal rating
Core inlet temp. (K)	316.7	316.7	316.5	0.06	0.06	High design basis temperature
Coolant flow to inner plenum (gpm)	2227	2228	2223	0.18	0.22	Low design basis flow
Coolant flow to outer plenum (gpm)	6487	6487	6477	0.15	0.15	Low design basis flow

4.2 Accident Analysis

4.2.1 Control Rod Withdrawal Startup Accident

A startup accident model has been developed using assumptions that are selected to maximize the reactivity insertion. The reactor is assumed to be initially critical at a power level of 100 W. Contrary to operating procedures and all previous training and experience, the operator is then assumed to withdraw the shim arms steadily without any pause, until the reactor is scrammed by a high power level trip. The accident model uses a reactivity insertion rate for the shim arm withdrawal equal to $5 \times 10^{-4}\,\Delta k/k$ per second. This rate is greater than the maximum measured and calculated rate at any shim arm position.

The power excursion is analyzed by using the RELAP5 point kinetics model. The positive reactivity ramp is terminated once a high power scram is initiated. Upon reactor scram the shim arms are assumed to insert from their initial critical positions of 22.6º and 41º (fully withdrawn) for the SU and the EOC conditions, respectively. For conservatism the calculation does not consider any fuel or moderator reactivity feedback. The high power level trip is set to 26 MW (130% of nominal operating power). This is conservative because the limiting safety system setting is actually at 125% of the nominal power.

The transient reactor powers are plotted in Figure 6. As shown in the figure, the reactor power increases almost exponentially in both cases. The figure also shows that the power rises faster in the SU than in the EOC and the different

behavior of the power increase is caused by different neutron kinetic conditions in the two cases.

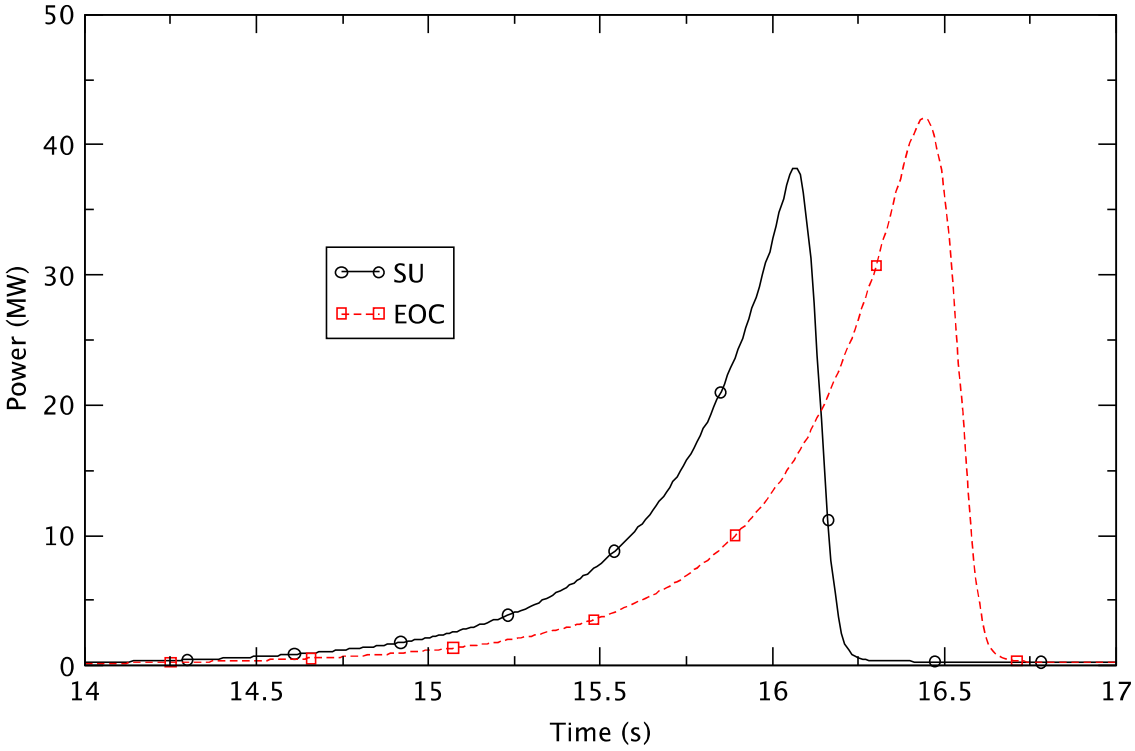

Figure 6 Reactor Power in Startup Accident with SU and EOC

Reactor trip occurs at around 16.03 and 16.35 s in the SU and EOC cases, respectively, about 0.1 s after the reactor power reaches 26 MW (due to delayed scram signal). The peak powers of 38.2 and 42.1 MW happen at 16.07 and 16.44 s in the SU and EOC cases, respectively. The differences in the magnitude and the timing of the peak power after reactor scram for the two cases are due to the lower rate of negative reactivity insertion for the EOC case as compared to that of the SU case. Figure 7 clearly illustrates the shim arm effect. It can be seen in the figure that the reactivity insertion rate is smaller at EOC than at SU because the shim arms drop from 41° in the former case while they drop from 22.6° in the latter case after a reactor scram. The initial smaller negative reactivity insertion rate delays the shutdown of the reactor in the EOC case, as compared to the SU case, giving more time for the positive reactivity ramp to raise the power further.

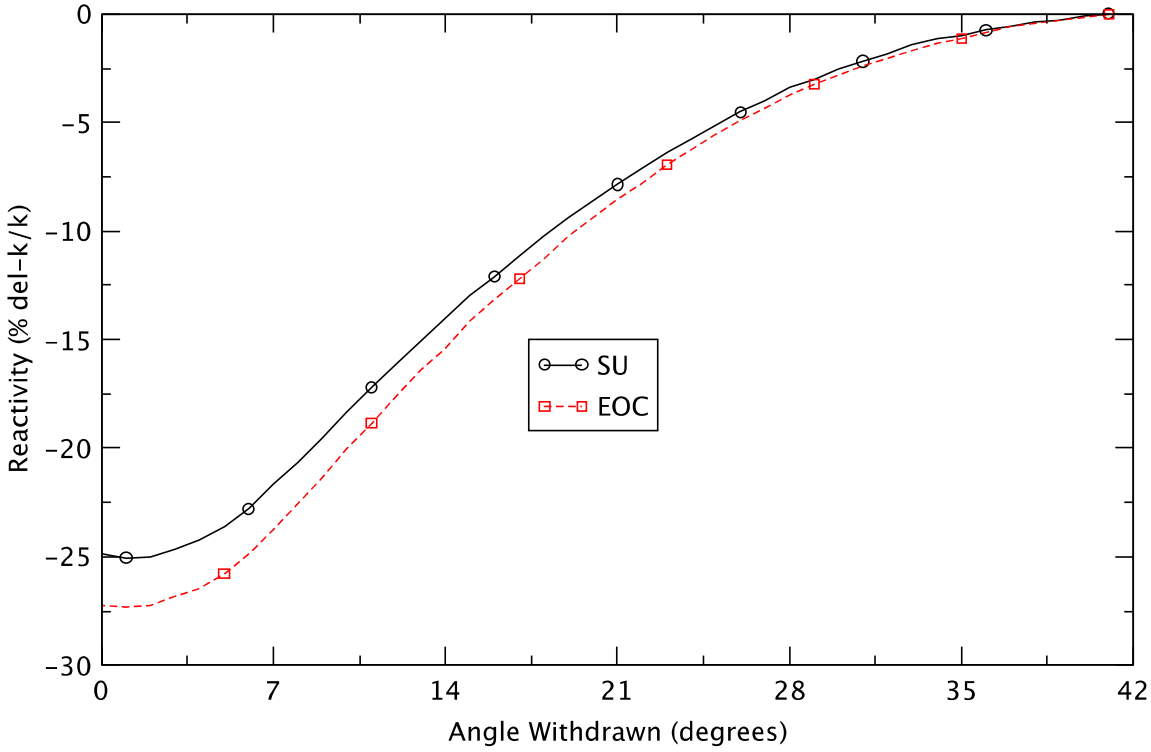

Figure 7 Shim Arm Worths as a Function of Angle Withdrawn

Minimum CHFRs are evaluated and shown in Figure 8. As depicted in Figure 8, CHFRs decrease until minimum CHFRs occur at 16.1 and 16.5 s and they are 2.213 in the SU and 2.064 in the EOC, respectively. They then continue increasing. Cuadra et al. (Cuadra et al., 2011) conducted a statistical analysis with a large size of sampling to quantify uncertainties of key parameters of CHF and discussed that minimum CHFRs would have to be larger than 1.4 to assure with 95% probability that there is no CHF in the high enriched uranium (HEU) NBSR. They also showed that the minimum CHFR needs to be larger than 1.8 in order for CHF not to happen with probability higher than 99.9%. Therefore, the calculated minimum CHFRs of 2.213 and 2.064 are above 1.8 and it indicates that the NBSR reactor is safe in the startup accidents with the SU and EOC power distributions.

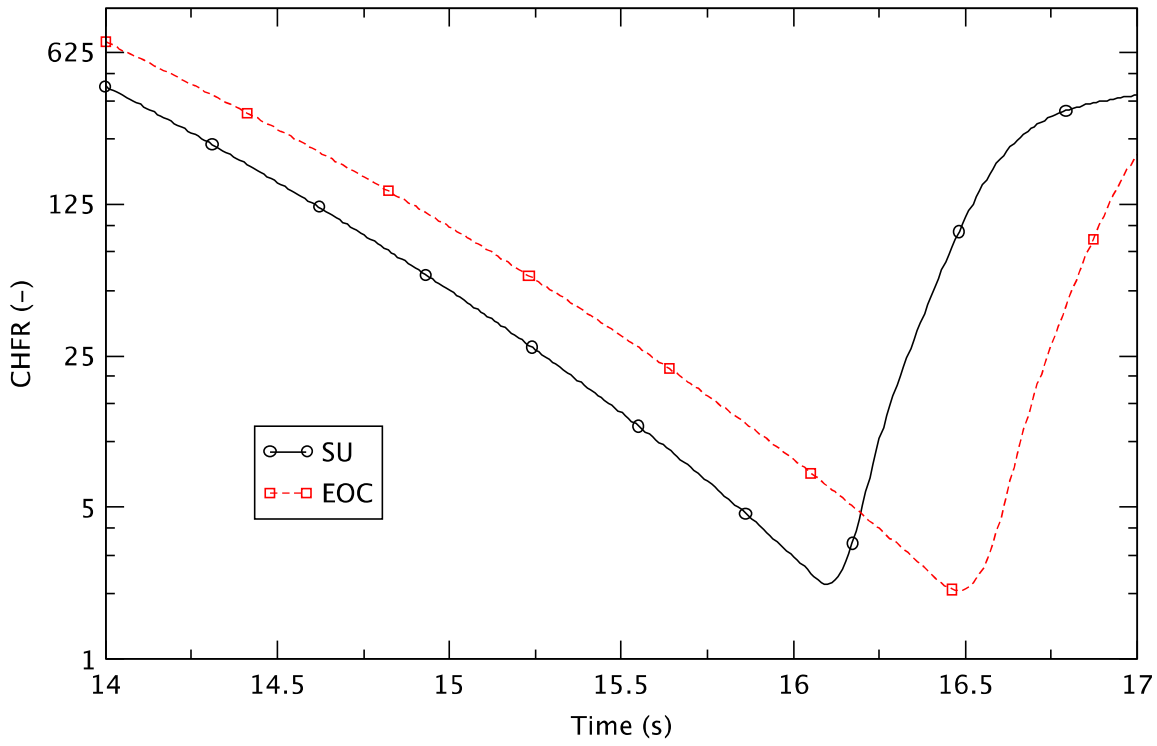

Figure 8 Critical Heat Flux Ratios in Startup Accident

Figure 9 illustrates cladding temperature behavior at the nodes where the minimum CHFR occurs. The temperature behavior is similar to that of the reactor power. The cladding temperature increases until it reaches 388.0 K at 16.1 s at SU and 392.3 K at 16.5 s at EOC, respectively, and then continues decreasing. The initial temperatures are 307.3 K. There are cladding temperature increases of 80.7 and 85.0 K at SU and EOC, respectively, and they appear not to be large. This, along with the large values of the minimum CHFRs, confirms that the integrity of fuel elements is preserved in both cases.

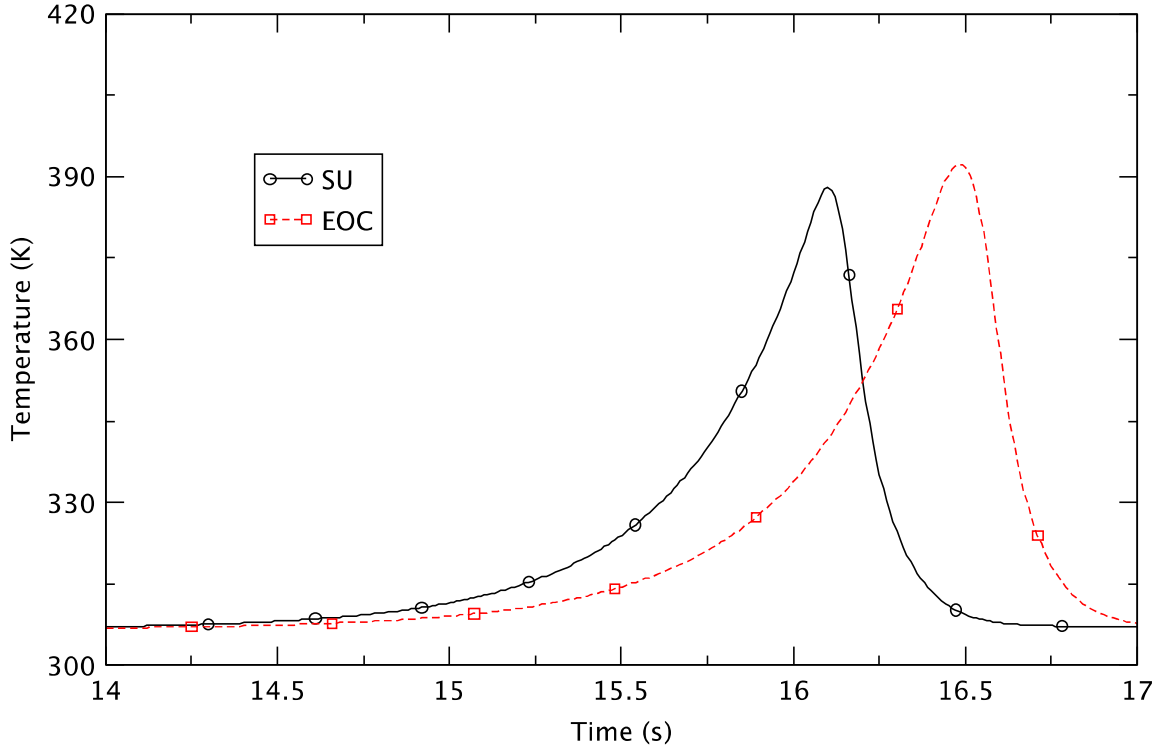

Figure 9 Cladding Temperature Behavior at Minimum CHFR Nodes in Startup Accident

4.2.2 Maximum Reactivity Insertion Accident

The maximum reactivity accident power excursion is also analyzed by using the RELAP5 point kinetics model. For conservatism the calculation does not consider any fuel or moderator reactivity feedback. For this accident a ramp reactivity insertion of 0.005 Δk/k is assumed to occur in 0.5 s. Except for this ramp reactivity insertion, the analysis methodology is the same as the one used for the startup accident.

The transient reactor powers are plotted in Figure 10. The reactor power increases from the beginning in both cases. The figure also shows that the power rises slightly faster at SU than at EOC and again the different behavior of the power increase is caused by different neutron kinetic conditions in the two cases.

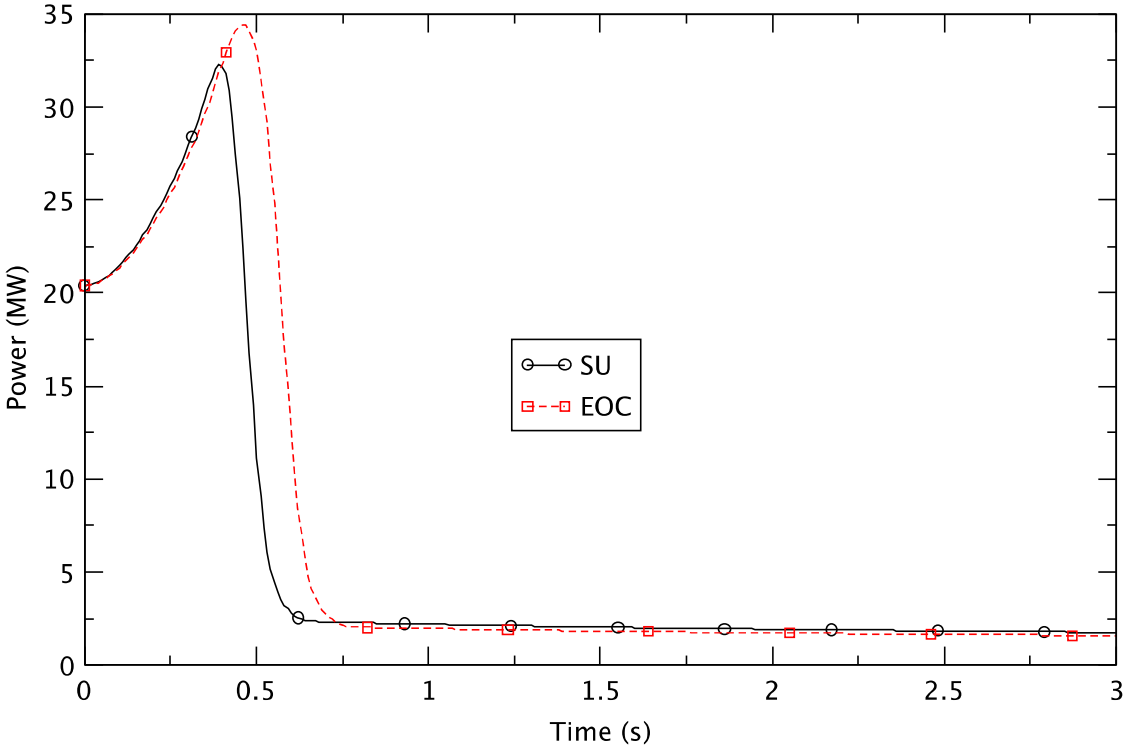

Figure 10 Reactor Power in Maximum Reactivity Insertion Accident with SU and EOC

Reactor trip occurs at 0.36 and 0.37 s in the SU and EOC cases, respectively, about 0.1 s after the reactor power reaches 26 MW due to delayed scram signal. The peak powers of 32.3 and 34.4 MW happen at 0.39 and 0.46 s at SU and EOC, respectively. It can be observed that the peak power is larger and occurs later after the reactor trip at EOC rather than at SU as observed in the startup accident.

As depicted in Figure 11, CHFRs decrease initially and minimum CHFRs occur at 0.42 and 0.50 s and they are 2.363 at SU and 2.338 at EOC, respectively. They then continue increasing. As discussed earlier, the minimum CHFR should be higher than 1.4 in order for CHF not to take place with probability higher than 95% or 1.8 with probability higher than 99.9%. The calculated minimum CHFRs of 2.363 and 2.338 indicate that the NBSR reactor is safe in the accidents of maximum reactivity insertion at SU and EOC.

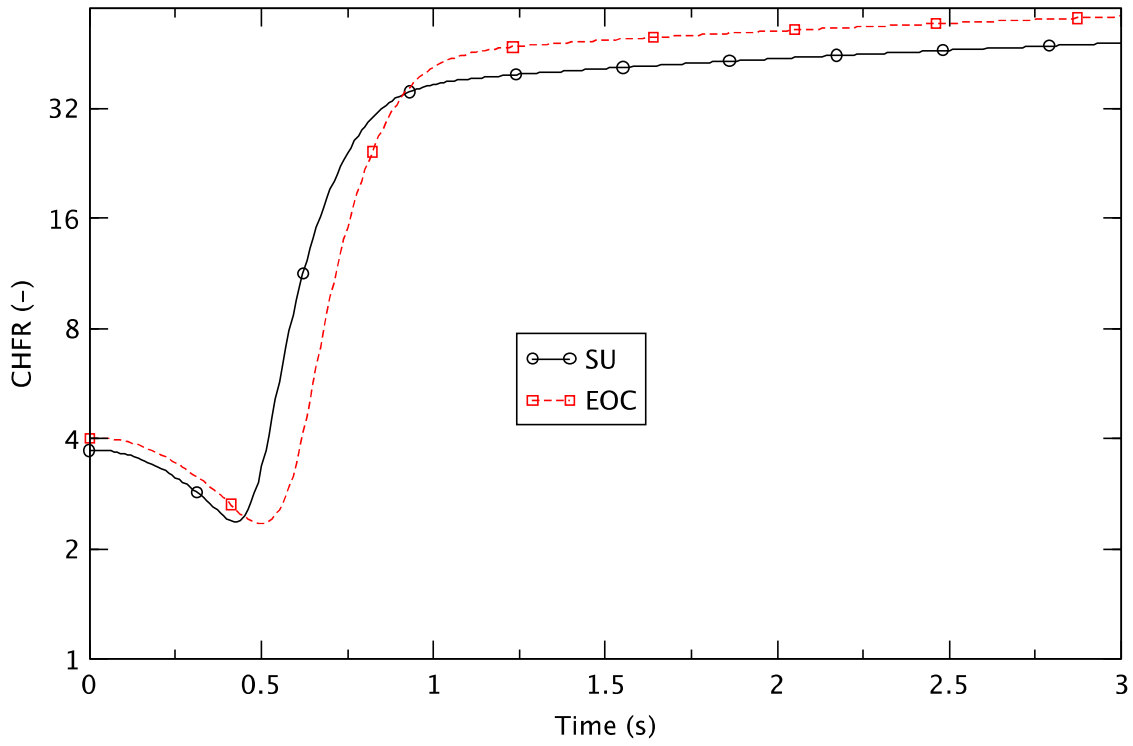

Figure 11 Critical Heat Flux Ratios in Maximum Reactivity Insertion Accident

Figure 12 illustrates cladding temperature behavior at the nodes where the minimum CHFR occurs. The temperature behavior is similar to the reactor power behavior. The cladding temperature increases until it reaches 386.8 K at 0.43 s at SU and 387.6 K at 0.50 s at EOC, respectively, and then continues decreasing. The SU and EOC initial cladding temperatures are 366.3 and 363.0 K, respectively. There are cladding temperature increases of 20.5 and 24.6 K at SU and EOC, respectively, and they appear to be small. This, along with the large values of the minimum CHFRs, confirms that the integrity of fuel elements is preserved in both cases.

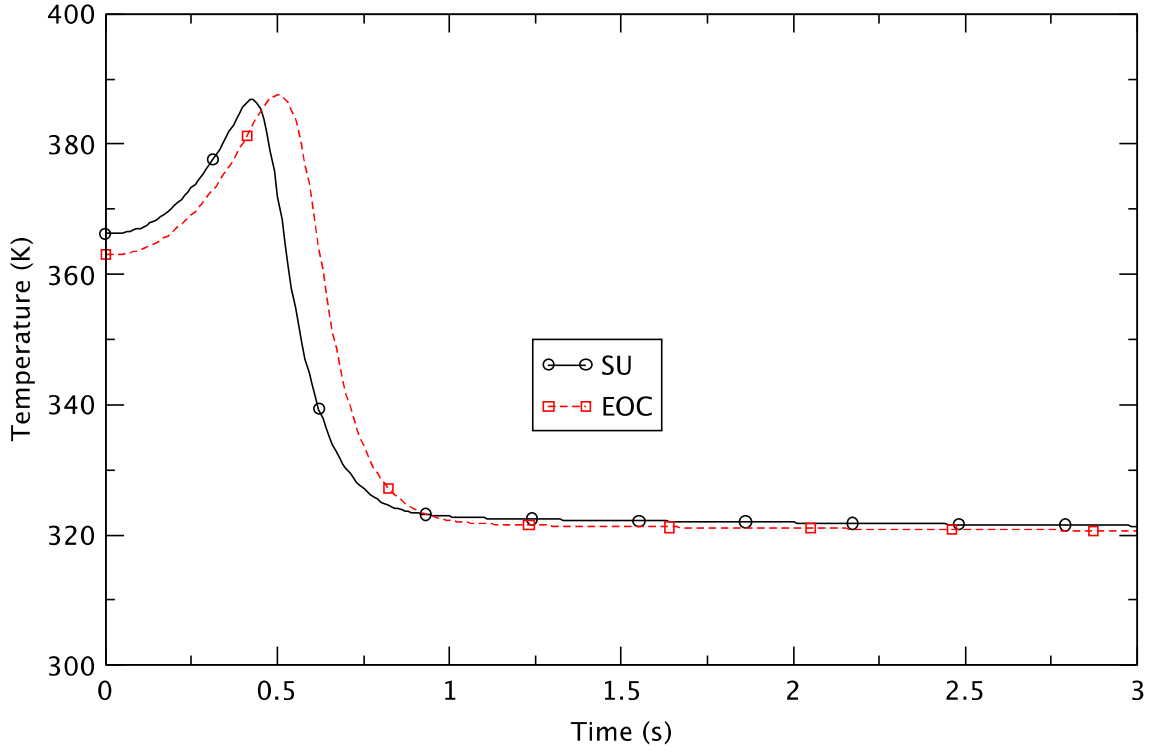

Figure 12 Cladding Temperature Behavior at Minimum CHFR Nodes in Maximum Reactivity Insertion Accident

5. *Conclusions*

A detailed RELAP5 model has been developed to analyze the NIST research reactor. Two postulated accidents have been simulated: constant rod withdrawal startup accident and maximum reactivity insertion accident. Two limiting points in a fuel cycle have been considered; namely, startup and end-of-cycle. Post-processing has been performed to evaluate CHF, CHFR, and minimum CHFR by developing a FORTRAN program. Reactor power, peak cladding temperature, and minimum CHFR have been examined in detail.

The evaluated minimum CHFRs are higher than 1.8 in all cases and indicating that the probability is higher than 99.9% that the NBSR reactor is safe without CHF occurring. It has been observed that the increases of the cladding temperatures are small. These analysis results confirm that the integrity of fuel elements is preserved in all cases.

Acknowledgments

This work was supported by the National Institute of Standards and Technology (NIST) and the NIST Center for Neutron Research (NCNR). The authors appreciate the cooperation of Sean O'Kelly and his staff at the NCNR.

Nomenclature

A Flow area (m^2)

A_H Heated area (m^2)
C_{pl} Specific heat at constant pressure of the liquid (kJ/kg.K)
W Channel width of rectangular channel (m)
G Mass flux ($kg/m^2.s$)
g Acceleration of gravity (m/s^2)
h_{fg} Latent heat of evaporation (kJ/kg)
q Heat flux

Greek Letter

σ Surface tension (N/m)
λ Critical wave length (m)
ρ Density of gas and liquid (kg/m^3)

Superscripts

* Dimensionless value

Subscripts

CHF Critical heat flux
RELAP5 RELAP5 prediction
g Gas phase
in Inlet
l Liquid phase
o Outlet
sub Subcooling

References

Becker, D.A., "30 Years of Reactor Characterization on the NBSR," Journal of Radioanalytical and Nuclear Chemistry, Vol. 244, No. 2, pp. 361-365, 2000.

Cheng, L., Hadson, A., Diamond, D., Xu, J., Carew, J., and Rorer, D., "Physics and Safety Analysis for the NIST research Reactor," BNL Technical Report, BNL-NIST-0803, Rev. 1, Brookhaven National Laboratory, April 2004.

Cuadra, A. and Cheng, L.Y., "Statistical Hot Channel Analysis for the NBSR," BNL Memo, Brookhaven National Laboratory, May 2011.

Kaminaga, M., Yamamoto, K., and Y. Sudo, "Improvement of Critical Heat Flux Correlation for Research Reactors using Plate-Type Fuel," J. Nucl. Sci. Technol. 35[12], pp. 943-951, 1998.

Hanson, A.L. and Diamond, D.J., "A Neutronics Methodology for the NIST Research Reactor Based on MCNPX," Proceedings of ICONE19 19th International Conference on Nuclear Engineering, Chiba, Japan, May 16-19, 2011.